Striatal Cholinergic Interneurons Control Motor Behavior and Basal Ganglia Function in Experimental Parkinsonism

Nicolas Maurice, Martine Liberge, Florence Jaouen, Samira Ztaou, Marwa Hanini, Jeremy Camon, Karl Deisseroth, Marianne Amalric, Lydia Kerkerian-Le Goff, Corinne Beurrier

Report

Cell Reports

Striatal Cholinergic Interneurons Control Motor Behavior and Basal Ganglia Function in Experimental Parkinsonism

Graphical Abstract

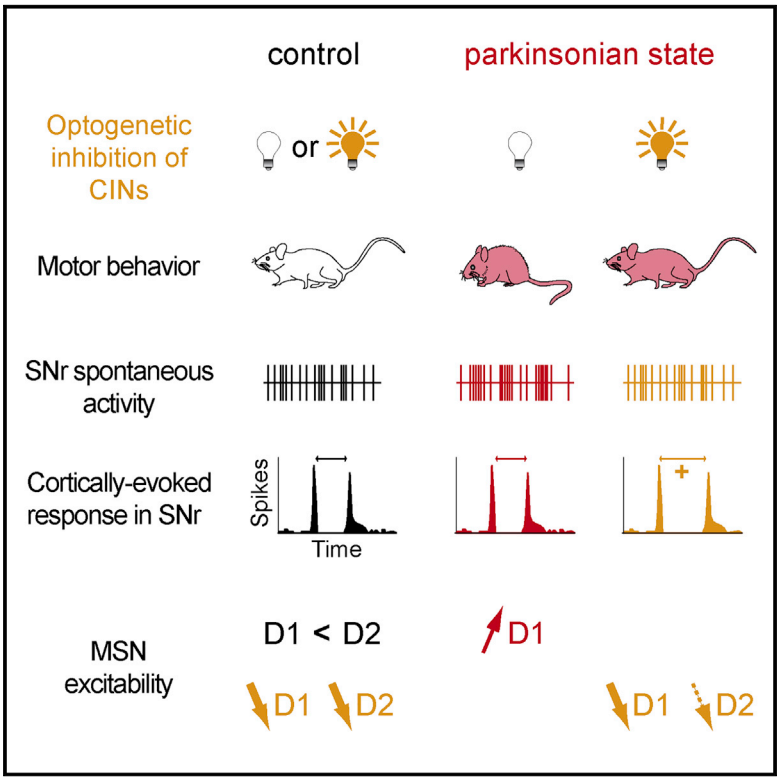

Authors

Nicolas Maurice, Martine Liberge, Florence Jaouen, ..., Marianne Amalric, Lydia Kerkerian-Le Goff, Corinne Beurrier

Correspondence

corinne.beurrier@univ-amu.fr

In Brief

By combining optogenetics with behavioral and electrophysiological approaches in mice, Maurice et al. provide evidence for a causal role of striatal cholinergic interneurons in parkinsonian symptomatology and identify underlying neural substrates in the basal ganglia network.

Highlights

- CIN activity impacts motor function and basal ganglia output in parkinsonian state
- CIN inhibition alleviates parkinsonian symptoms, while activation has no effect
- CIN inhibition corrects burst firing and enhances cortically evoked inhibition in SNr
- CIN's control of D2-, but not D1-MSN, excitability is reduced in parkinsonian state

Maurice et al., 2015, Cell Reports *13*, 657–666
October 27, 2015 ©2015 The Authors
http://dx.doi.org/10.1016/j.celrep.2015.09.034

Cell Reports
Report

Striatal Cholinergic Interneurons Control Motor Behavior and Basal Ganglia Function in Experimental Parkinsonism

Nicolas Maurice,[1,4] Martine Liberge,[2,4] Florence Jaouen,[1] Samira Ztaou,[2] Marwa Hanini,[1] Jeremy Camon,[2] Karl Deisseroth,[3] Marianne Amalric,[2,5] Lydia Kerkerian-Le Goff,[1,5] and Corinne Beurrier[1,5,*]
[1]Aix-Marseille Université (AMU), Centre National de la Recherche Scientifique (CNRS), UMR 7288, Institut de Biologie du Développement de Marseille (IBDM), 13288 Marseille cedex 9, France
[2]Aix-Marseille Université (AMU), Centre National de la Recherche Scientifique (CNRS), UMR 7291, FR3C 3512, Laboratoire de Neurosciences Cognitives, 13331 Marseille cedex 3, France
[3]Departments of Bioengineering and Psychiatry and Howard Hughes Medical Institute, Stanford University, Palo Alto, CA 94305, USA
[4]Co-first author
[5]Co-senior author
*Correspondence: corinne.beurrier@univ-amu.fr
http://dx.doi.org/10.1016/j.celrep.2015.09.034

SUMMARY

Despite evidence showing that anticholinergic drugs are of clinical relevance in Parkinson's disease (PD), the causal role of striatal cholinergic interneurons (CINs) in PD pathophysiology remains elusive. Here, we show that optogenetic inhibition of CINs alleviates motor deficits in PD mouse models, providing direct demonstration for their implication in parkinsonian motor dysfunctions. As neural correlates, CIN inhibition in parkinsonian mice differentially impacts the excitability of striatal D1 and D2 medium spiny neurons, normalizes pathological bursting activity in the main basal ganglia output structure, and increases the functional weight of the direct striatonigral pathway in cortical information processing. By contrast, CIN inhibition in nonlesioned mice does not affect locomotor activity, equally modulates medium spiny neuron excitability, and does not modify spontaneous or cortically driven activity in the basal ganglia output, suggesting that the role of these interneurons in motor function is highly dependent on dopamine tone.

INTRODUCTION

Parkinson's disease (PD) is a debilitating neurodegenerative movement disorder resulting from the loss of nigral dopaminergic (DA) neurons that project massively to the striatum, the main basal ganglia input structure. The hypokinetic parkinsonian syndrome is thought to be the consequence of opposite changes in the activity of the two populations of GABAergic striatal projection neurons, also called medium spiny neurons (MSNs), which control the basal ganglia output nuclei, mainly the substantia nigra pars reticulata (SNr) in rodent. Dopamine D1 receptor-expressing MSNs (D1 or direct MSNs), giving rise to a monosynaptic inhibitory projection (direct pathway) onto SNr, become hypoactive, whereas dopamine D2 receptor-expressing MSNs (D2 or indirect MSNs), at the origin of a polysynaptic projection with excitatory influence onto SNr (indirect pathway), become hyperactive (Albin et al., 1989; Mallet et al., 2006). This imbalance leads to pathological activation of SNr, reinforcing its inhibitory tone onto the thalamocortical circuit and, hence, on motor cortical outflow. The pathological changes in the activity of the two striatal pathways, whose functional relationship with movement control is still debated (Calabresi et al., 2014; Cui et al., 2013), may involve profound reorganizations within the striatal circuitry.

Striatal cholinergic interneurons (CINs), which correspond to the tonically active neurons recorded in vivo, constitute 1%–3% of all striatal neurons. Despite being few in numbers, they are the main source of acetylcholine (ACh) within the striatum, and their dense terminal fields are primarily directed to MSNs (Phelps et al., 1985). The improvement of parkinsonian tremor by both DA agonists and anticholinergic drugs led to the DA-ACh balance hypothesis, where DA and ACh are believed to play opposite roles in the striatum (Barbeau, 1962). This clinical observation particularly underlines the functional impact of ACh as DA levels fall. There is indeed compelling evidence showing that DA depletion triggers complex alterations in striatal cholinergic signaling and activity (Aosaki et al., 1994; Ding et al., 2006), leading, among other things, to morphofunctional alterations of striatal output neurons (Pisani et al., 2007; Shen et al., 2007). However, whether and how this cholinergic-dependent disruption of striatal properties contributes to motor symptoms in PD and affects basal ganglia circuitry remain an open question.

The diversity of cholinergic receptors expressed in the striatum, located both at the presynaptic and postsynaptic levels (Goldberg et al., 2012), suggests that CINs exert complex and powerful influence on striatal functioning and, hence, on basal ganglia outflow. An additional level of complexity in understanding cholinergic regulation of striatal function comes from recent studies showing the following: (1) CINs co-release glutamate able to evoke fast glutamatergic responses in MSNs (Higley

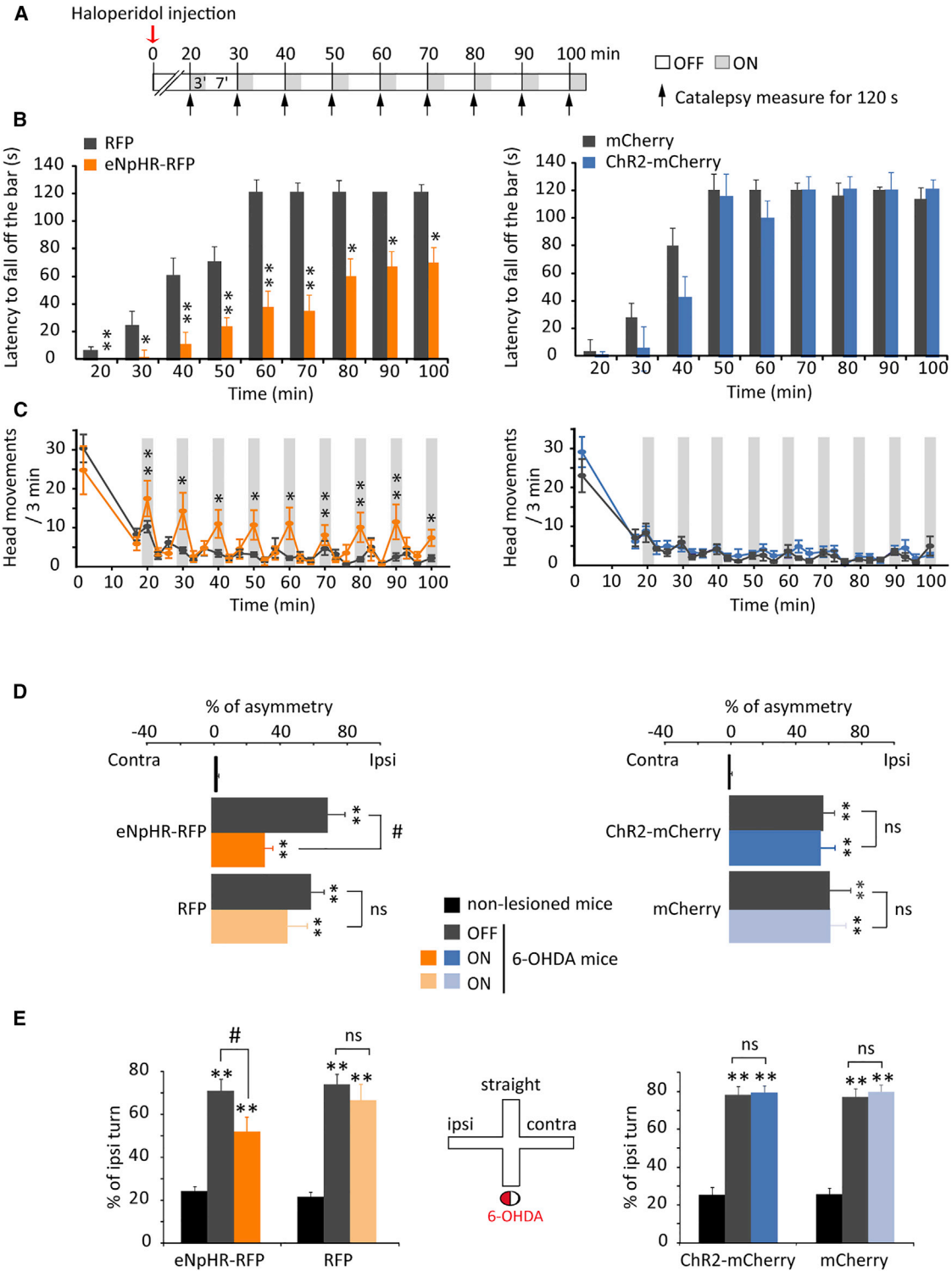

Figure 1. Photoinhibition of CINs rReduces Haloperidol-Induced Catalepsy and Relieves Parkinsonian-like Motor Deficits

(A) Experimental design. Mice received haloperidol (0.25 mg/kg) and the latency to step down the bar was measured 20 min later, then every 10 min, with a 120-s cutoff. Light was turned on (blue light: 10 Hz, 25-ms pulse width; yellow light: continuous illumination) for 3 min when placing the mice on the bar and was turned off afterward for 7 min, until next measure.

(B) Yellow light reduced haloperidol-induced catalepsy in eNpHR-RFP mice versus RFP mice (*$p < 0.05$, **$p < 0.01$, U-Mann-Whitney after significant Kruskal-Wallis test), whereas blue light illumination in ChR2-mCherry mice had no effect versus mCherry mice ($p = 0.3$).

(legend continued on next page)

et al., 2011), (2) CIN activation can drive GABA release from dopaminergic terminals (Nelson et al., 2014; Tritsch et al., 2014) and neuroptide Y-expressing interneurons (English et al., 2011), and (3) their synchronous activation triggers striatal DA release (Threlfell et al., 2012). While we do not know yet how these different actions are coordinated in vivo, these results suggest that DA/ACh interactions are more complex than the traditional antagonistic model would predict. Therefore, the contribution of CINs to basal ganglia function cannot be fully understood unless an approach mimicking the diversity of their actions is used. Optogenetics that allows precise control of circuit function, was, for example, used successfully to demonstrate the role of CINs in the nucleus accumbens during cocaine conditioning (Witten et al., 2010).

Here, using a combination of optogenetic, behavioral, and electrophysiological approaches, we demonstrate a major role of CINs in PD pathophysiology. We show that selective inhibition of CINs alleviates motor deficits and corrects dysfunctions at the main input and output stages of the basal ganglia network in PD mouse models, with a preferential action on the direct striatonigral pathway.

RESULTS

Inhibition of Striatal Cholinergic Interneurons Reduces Parkinsonian-like Motor Deficits

We expressed ChR2-mCherry or eNpHR-RFP in choline acetyltransferase (ChAT)-expressing neurons by injecting a Cre-dependent adeno-associated virus (AAV) carrying the opsins or their reporter genes into the dorsal striatum of $ChAT^{cre/cre}$ mice (subsequently referred to as ChR2-mCherry and eNpHR-RFP mice). Quantifying the proportion of neurons expressing opsins that were also ChAT positive and vice versa demonstrated the specificity and efficiency of the targeting strategy (Figure S1). Recordings of optogenetically identified CINs in striatal slices and anesthetized mice showed that opsins were functional (Figure S2).

CIN photoinhibition or photoactivation had no significant effect on locomotor activity of non-lesioned RFP, eNpHR-RFP, mCherry, and ChR2-mCherry mice in an open field (Figure S3A). To determine whether CINs affect parkinsonian akinesia, the effects of CIN modulation were examined in the haloperidol-induced catalepsy model (Figure 1A). The eNpHR-RFP haloperidol-treated mice removed their forepaws from the bar significantly faster under yellow illumination than did the RFP-treated mice (Figure 1B). Consistently, yellow light restored head movements in a light-locked manner in haloperidol-injected eNpHR-RFP mice, demonstrating a robust anti-akinetic action of CIN inhibition (Figure 1C). In contrast, ChR2-mCherry mice under blue illumination exhibited a long-lasting cataleptic state, similar to mCherry mice (Figures 1B and 1C).

We next tested whether CIN inhibition could alleviate motor dysfunction in the 6-hydroxydopamine (6-OHDA) lesional model of PD. Unilateral 6-OHDA injection into the substantia nigra pars compacta (SNc) resulted in a near-total loss of DA cells after 2 weeks. In the cylinder test (Figure 1D), RFP and mCherry non-lesioned mice used their two forepaws indifferently during exploratory rearing (asymmetry score close to zero). The 6-OHDA lesions produced a significant shift toward ipsilateral forepaw use due to contralateral forelimb akinesia. Photoinhibition of CINs ipsilateral to the lesioned side in eNpHR-RFP mice induced a significant reduction in the asymmetry score. In contrast, CIN photoactivation in ChR2-mCherry 6-OHDA mice did not affect asymmetry (Figure 1D). In the cross maze test (Figure 1E), the 6-OHDA-induced bias toward ipsilateral turns, which reflects sensorimotor neglect, was significantly reduced by CIN inhibition in eNpHR-RFP mice, while CIN activation had no effect in ChR2-mCherry mice. The non-selective muscarinic receptor antagonist scopolamine (1 mg/kg) also reduced the asymmetry in the cylinder and cross maze tests in 6-OHDA mice (Figures S3B and S3C). Finally, we examined the effect of CIN photoinhibition on L-DOPA-induced dyskinesia, a main side effect of long-term DA treatment. CIN inhibition in eNpHR-RFP mice failed to affect the severity of dyskinesia once expressed (Figure S4). Taken together, these data show that CIN inhibition has no effect on spontaneous locomotion and L-DOPA-induced dyskinesia in our lesion and treatment conditions, but significantly alleviates parkinsonian-like motor deficits.

Inhibition of Striatal CINs Regulates the Basal Ganglia Output Structure in Parkinsonian Condition Only

A leading hypothesis on the origin of motor dysfunction in PD is that DA loss induces abnormal bursting activity in basal ganglia output nuclei, leading to pathological inhibitory tone onto the thalamocortical circuit that disrupts motor planning and execution. We tested whether striatal CIN inhibition modifies the activity of SNr neurons recorded in vivo in anesthetized transgenic eNpHR mice. CIN photoinhibition in non-lesioned animals did not affect spontaneous activity of SNr neurons (Table S1). The 6-OHDA mice showed altered burst firing, with significant increases in burst duration and number of spikes per burst (Figure 2A). CIN photoinhibition normalized these changes, without

(C) Light partially restored head movements in eNpHR-RFP mice (ON versus OFF preceding light: *$p < 0.05$, **$p < 0.01$, paired Student's t test after significant two-way ANOVA), but not in ChR2-mCherry mice or in control RFP and mCherry mice (n = 10–13 per group).
(D) In the cylinder test, 6-OHDA mice showed marked forelimb asymmetry compared to non-lesioned mice (**$p < 0.01$, Fisher's least significant difference [LSD] test after significant ANOVA). (Left) This asymmetry was significantly improved by yellow light in eNpHR-RFP mice (ON versus OFF: #$p < 0.05$, Student's t test). Light did not affect asymmetry in RFP control mice (n = 7–8 per group). (Right) The significant forelimb asymmetry measured in 6-OHDA versus non-lesioned mice (**$p < 0.01$, Fisher's LSD test after significant ANOVA) was not affected by blue light illumination in ChR2-mCherry (ON versus OFF: ns, Student's t test) and mCherry (ON versus OFF: ns, Student's t test) mice (n = 7–8 per group).
(E) (Left) Ipsilateral turn bias induced by 6-OHDA lesion in the cross maze (6-OHDA versus non-lesioned: **$p < 0.01$, one-way ANOVA) was partially corrected by photoinhibition in eNpHR-RFP mice (ON versus OFF: #$p < 0.05$, paired Student's t test), but not in RFP control mice (n = 14 per group). (Right) Photoactivation did not affect the ipsilateral turn bias induced by 6-OHDA lesion (6-OHDA versus non-lesioned: **$p < 0.01$, one-way ANOVA) in ChR2-mCherry mice nor in mCherry mice (ON versus OFF: ns, Student's t test, n = 12 per group). In (D) and (E), continuous illumination was for 5 min with yellow light and 25-ms pulse width was at 10 Hz for blue light. Circle under the cross maze symbolizes a mouse with the 6-OHDA-injected side in red. Errors bars, SEM.

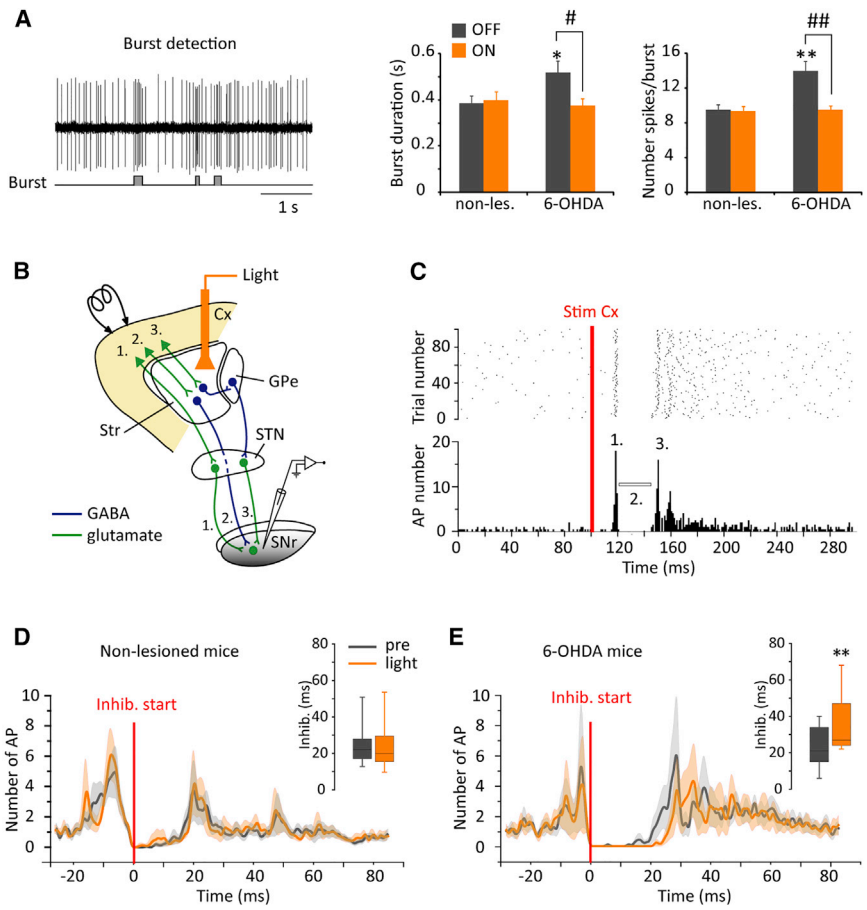

Figure 2. Photoinhibition of CINs Normalizes SNr Burst Firing and Strengthens the Inhibitory Influence of the Striatonigral Direct Pathway in 6-OHDA Mice

(A) Detection of bursts according to Poisson Surprise analysis in a spontaneously firing SNr neuron recorded in 6-OHDA transgenic eNpHR mice. The histograms show that the 6-OHDA induced increases in burst duration and number of spikes per burst (6-OHDA versus non-lesioned: *$p < 0.05$, **$p < 0.01$, Student's t test) were normalized by CIN photoinhibition (light was delivered for 1 min; 6-OHDA ON versus OFF: #$p < 0.05$, ##$p < 0.01$, Holm-Sidak test after significant one-way ANOVA). Non-lesioned mice, n = 18 cells from six mice; 6-OHDA mice, n = 13 cells from six mice.

(B) Schematic representation shows pathways activated by cortical stimulation that project to SNr neurons. Cx, cortex; Str, striatum; GPe, external globus pallidus; STN, subthalamic nucleus.

(C) Raster plot and peristimulus time histogram (PSTH) show the typical triphasic response evoked by motor cortex stimulation in one SNr neuron recorded from a 6-OHDA transgenic eNpHR mouse.

(D and E) Population PSTHs of the cortically evoked responses recorded in SNr neurons in non-lesioned (D, n = 17 cells from six mice) and 6-OHDA (E, n = 7 cells from five mice) mice. The same neuron was recorded before (pre, gray line) and during (light, orange line) CIN photoinhibition. Light was delivered for 1 s at the beginning of each trial. PSTHs are aligned on the beginning of the inhibitory component (red lines) and the light-shaded colors represent SEM. CIN photoinhibition induced a significant increase of the inhibitory component duration only in 6-OHDA mice, as illustrated by the box plots (insets) (**$p < 0.01$, Holm-Sidak test after significant one-way RM ANOVA). Errors bars, SEM.

modifying the parameters unaltered by the lesion (firing frequency and burst recurrence) (Table S1).

Next, to examine whether CINs influence the processing of cortical information through the trans-striatal pathways, we recorded the responses of individual SNr neurons to cortical stimulation (Figures 2B and 2C). As previously reported, such stimulation triggers a complex response composed, in most cases, of an early excitation followed by an inhibition and a late excitation, which has been attributed to the respective activation of the hyperdirect corticosubthalamic, the direct and indirect striatonigral pathways (Maurice et al., 1999; Ryan and Sanders, 1994; Sano et al., 2013; Tachibana et al., 2008). Because the characteristics of the evoked responses greatly vary among cells depending on the stimulation (e.g., location and number of stimulated fibers) but remain stable in a given cell over time, comparisons were made for a same cell under successive light conditions and not between cells from 6-OHDA versus non-lesioned mice. CIN photoinhibition had no effect on cortical information transfer in non-lesioned mice, whereas, in 6-OHDA mice, it increased the duration of the inhibitory component of the triphasic response without significantly affecting the excitatory components (Figures 2D and 2E; Table S2). Since parkinsonian akinesia is classically associated with overactive indirect pathway and hypoactive direct pathway, our results suggest that CIN inhibition might partially restore balance in striatal outputs by increasing the functional impact of the direct pathway. In contrast, CIN photoinhibition had no effect on SNr spontaneous activity and cortical information transfer in non-lesioned transgenic eNpHR mice.

Dopamine Depletion Affects the Intrinsic Excitability of D1 MSNs

We first determined whether CINs themselves were affected by 6-OHDA lesion, as there is no consensus on whether CIN activity or striatal ACh release increases in PD models. Optogenetically identified CINs recorded either in slices or in anesthetized mice exhibited similar firing frequency in non-lesioned and 6-OHDA conditions (Figure 3), showing that they are not hyperactive in our experimental conditions. However, CINs were more excitable in slices from 6-OHDA mice, as illustrated by a lower rheobase current (non-lesioned: 137.7 ± 16.7 pA, n = 17; 6-OHDA: 87.1 ± 16.5 pA, n = 17; $p < 0.05$, Mann-Whitney test).

We then tested whether CIN modulation of striatal functions could be altered in PD state, by examining its impact on identified D1 and D2 MSNs that form the direct and indirect striatal projection systems, 2–3 weeks after 6-OHDA lesion. The

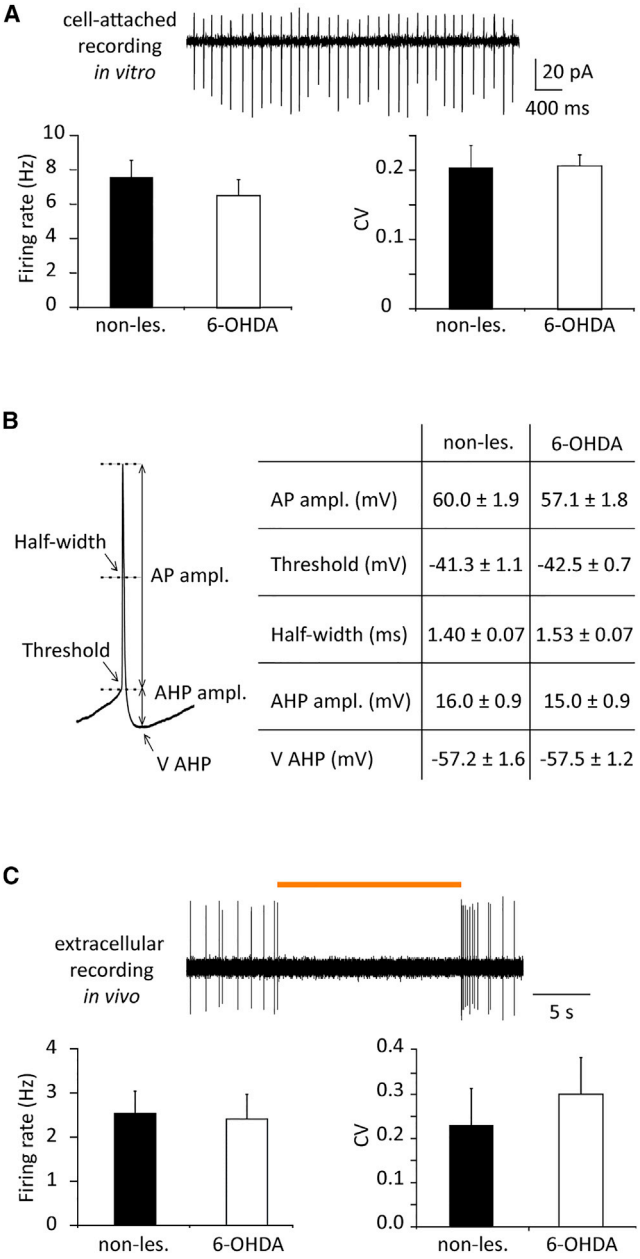

	non-les.	6-OHDA
AP ampl. (mV)	60.0 ± 1.9	57.1 ± 1.8
Threshold (mV)	-41.3 ± 1.1	-42.5 ± 0.7
Half-width (ms)	1.40 ± 0.07	1.53 ± 0.07
AHP ampl. (mV)	16.0 ± 0.9	15.0 ± 0.9
V AHP (mV)	-57.2 ± 1.6	-57.5 ± 1.2

Figure 3. Impact of 6-OHDA Lesion on CIN Electrophysiological Properties

(A) Spontaneous activity from a CIN recorded in cell-attached configuration. Histograms show the mean firing rate and coefficients of variation (CV = firing rate SD/firing rate mean) in non-lesioned (n = 12 cells) and 6-OHDA (n = 20 cells) transgenic eNpHR mice (ns, Mann-Whitney test).

(B) Action potential characteristics of CINs recorded in non-lesioned (n = 13 cells) and 6-OHDA (n = 22 cells) mice. No significant differences were observed between the two groups (ns, Student's t test).

(C) Spontaneous activity and optogenetic identification of a CIN recorded in vivo. Histograms show the mean frequency rate and CVs (firing rate SD/firing rate mean) in non-lesioned (n = 8 cells) and 6-OHDA (n = 7 cells) transgenic eNpHR mice (ns, Mann-Whitney test). Errors bars, SEM.

resting membrane potentials of D1 and D2 MSNs were similar in non-lesioned and 6-OHDA mice (data not shown). However, in non-lesioned mice, D2 MSNs were more excitable than D1 MSNs, in agreement with previous reports (Gertler et al., 2008; Kreitzer and Malenka, 2007; Figure 4A). After DA depletion, D2 MSN excitability was not changed, while that of D1 MSNs greatly increased. D1 MSNs fired at higher frequency at each depolarizing current step, and the rheobase current was significantly lower in 6-OHDA versus non-lesioned mice (Figure 4). These results show that DA depletion reduces the dichotomy between D1 and D2 MSN excitability by increasing D1 MSN excitability.

Striatal CINs Differentially Modulate the Excitability of D1 and D2 MSNs in Parkinsonian Condition

Changes in intrinsic membrane excitability can occur either independently or in concert with changes in synaptic inputs. As cortical inputs strongly drive MSN activity and are modulated by presynaptic muscarinic receptors (Hernández-Echeagaray et al., 1998; Malenka and Kocsis, 1988; Pakhotin and Bracci, 2007), we investigated whether CIN inhibition affects corticostriatal transmission. Recordings were made 2–3 weeks after 6-OHDA lesion in transgenic eNpHR/D1 mice expressing both eNpHR in CINs and the fluorescent reporter tdTomato in DA D1 receptor-containing neurons (Figure S5A). In non-lesioned mice, excitatory postsynaptic currents (EPSCs) were not significantly altered by CIN inhibition, both in D1 and D2 MSNs (D1 MSNs, light versus pre-light: 325.99 ± 57.92 pA versus 311.16 ± 53.47 pA, not significant [ns], paired Student's t test, n = 14 cells; D2 MSNs, light versus pre-light: 214.98 ± 30.07 pA versus 214.59 ± 26.44 pA, ns, paired Student's t test, n = 11 cells) (Figure S5B). In contrast, CIN inhibition in 6-OHDA mice significantly potentiated EPSCs in both D1 and D2 MSNs (D1 MSNs, light versus pre-light: 262.22 ± 24.93 pA versus 240.76 ± 23.84 pA, $p < 0.05$, Wilcoxon test, n = 15 cells; D2 MSNs, light versus pre-light: 231.06 ± 34.00 pA versus 198.06 ± 24.07 pA, $p < 0.05$, Wilcoxon test, n = 9 cells) (Figure S5B). This potentiation was blocked by scopolamine (10 μM) (data pooled for D1 and D2 MSNs: light versus pre-light: 181.24 ± 35.92 pA versus 178.31 ± 33.35 pA, ns, paired Student's t test, n = 8 cells, data not shown). These results show that CIN inhibition potentiates corticostriatal transmission onto both D1 and D2 MSNs in parkinsonian condition. Therefore, corticostriatal transmission is unlikely to contribute to a differential impact of CIN inhibition on D1 and D2 MSNs.

In the healthy striatum, cholinergic modulation facilitates the firing of MSNs through M1 receptors (Galarraga et al., 1999; Goldberg et al., 2012; Pisani et al., 2007). What happens after chronic DA depletion is still unclear. We therefore examined whether and how CIN photoinhibition impacts MSN excitability in non-lesioned and 6-OHDA mice. D1 and D2 MSNs fired significantly less action potential during light illumination in both non-lesioned and 6-OHDA mice (Figures 5A and 5B). However, while the magnitude of firing inhibition was similar in D2 and D1 MSNs in non-lesioned mice, firing inhibition was weaker in D2 MSNs compared to D1 MSNs in 6-OHDA mice (Figure 5C). This result shows that D2 MSNs are less sensitive to CIN inhibition than D1 MSNs after DA depletion.

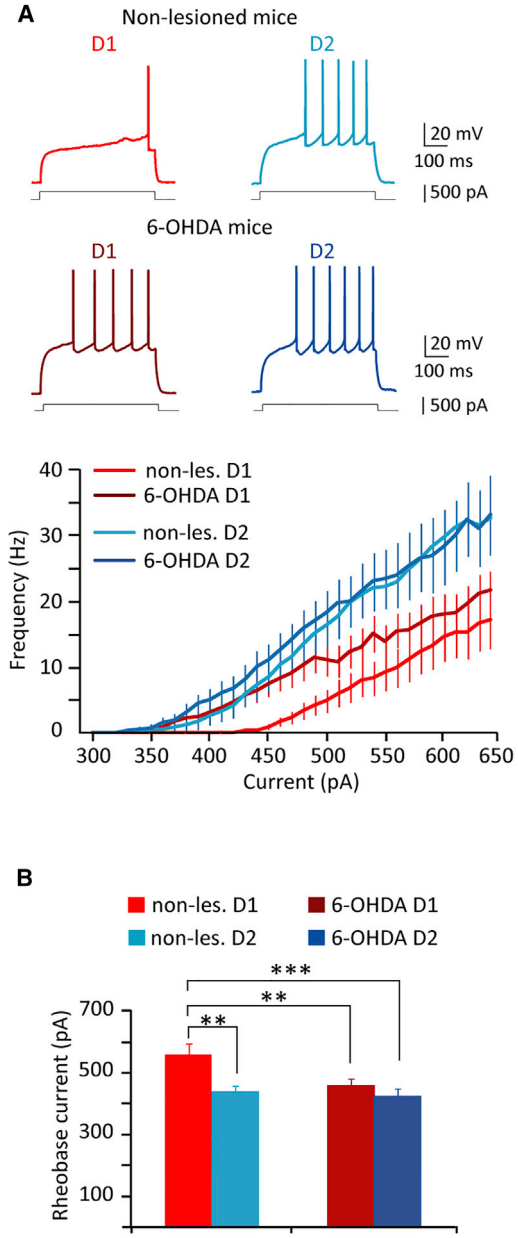

Figure 4. Impact of 6-OHDA Lesion on D1 and D2 MSN Excitability

(A) Current-clamp recordings showing the responses of D1 and D2 MSNs to depolarizing current pulses in non-lesioned (+450 pA) and 6-OHDA (+400 pA) mice. Summary graph illustrates the number of action potentials as a function of injected current in D1 MSNs (non-lesioned mice, n = 14 cells; 6-OHDA mice, n = 23 cells) and D2 MSNs (non-lesioned mice, n = 13 cells; 6-OHDA mice, n = 13 cells).

(B) Bars graph shows the mean rheobase current in D1 MSNs (non-lesioned mice, n = 14 cells; 6-OHDA mice, n = 23 cells) and D2 MSNs (non-lesioned mice, n = 13 cells; 6-OHDA mice, n = 13 cells) (**$p < 0.01$, ***$p < 0.001$, Holm-Sidak test after significant one-way ANOVA). Errors bars, SEM.

DISCUSSION

Although ACh is undeniably a critical player in striatal functioning, the role of CINs in PD pathophysiology has remained unsolved. We tackled this issue by combining optogenetics with in vitro and in vivo electrophysiology and behavioral analyses. We first showed that selective inhibition of CINs in the dorsal striatum reduces parkinsonian motor dysfunction in pharmacological and lesional PD models, attesting to their causal involvement in PD symptomatology. This provides a functional support for the long-standing hypothesis that poses PD as a striatal cholinergic disorder. Second, we identified several physiological parameters affected by CIN inhibition in the parkinsonian condition at both the input (striatum) and output (SNr) levels of the basal ganglia network. In addition, we found that CIN inhibition does not significantly impact basic motor function nor the spontaneous and cortically driven activity of SNr neurons in non-lesioned mice. This lack of effect in SNr is consistent with previous results from selective CIN ablation (Sano et al., 2013). Also, CIN inhibition does not modify the severity of dyskinesia in 6-OHDA mice. Altogether, these data suggest that CIN actions are highly dependent on DA tone.

CIN inhibition in vivo efficiently alleviates parkinsonian deficits measured after 6-OHDA lesions and neuroleptic-induced catalepsy, two different models widely used to assess motor symptoms reminiscent of parkinsonian akinesia. As neural correlates of PD symptoms' improvement by CIN inhibition, our in vivo recordings showed that it normalized the 6-OHDA-induced changes in SNr burst firing. Over the last few years, an abundant literature has clearly reported that parkinsonism is associated with increased bursting activity in the basal ganglia, including SNr (Lobb, 2014; Rivlin-Etzion et al., 2006; Wichmann et al., 1999). Even though the mechanisms leading to this abnormal activity are still elusive, its normalization by efficient antiparkinsonian treatments, such as dopatherapy or subthalamic nucleus deep brain stimulation (Brown, 2003; Degos et al., 2005; Eusebio et al., 2011), suggests that such change may contribute importantly to the development of the behavioral manifestations of the disease. Thus, it is likely that the decrease in burst activity of SNr neurons elicited by CIN inhibition contributes to the improvement of parkinsonian symptoms that we observed in 6-OHDA mice. Future studies will be required to understand fully how CINs influence SNr burst firing in PD.

The second effect of CIN inhibition revealed by our in vivo recordings in 6-OHDA mice was an increase in the inhibitory component of the cortically evoked triphasic response in SNr neurons, suggesting that CIN silencing strengthens the inhibitory influence of the direct striatonigral pathway in parkinsonian condition. Although the relationship between the activity of the direct and indirect pathways and movement generation is still under debate, it has been demonstrated that specific activation of D1 MSNs by optogenetics efficiently relieves parkinsonian deficits (Kravitz et al., 2010). In this context, it is likely that the increased duration of the cortically evoked inhibition induced by CIN inhibition contributes importantly to the improvement of parkinsonian-like motor symptoms induced by DA depletion.

What are the striatal targets modulated by CINs that could mediate their preponderant action on basal ganglia function in PD state? We showed that CIN inhibition in 6-OHDA mice potentiates corticostriatal transmission onto both types of MSNs. However, our recordings in the SNr of 6-OHDA mice clearly showed that CIN inhibition increases the cortically evoked

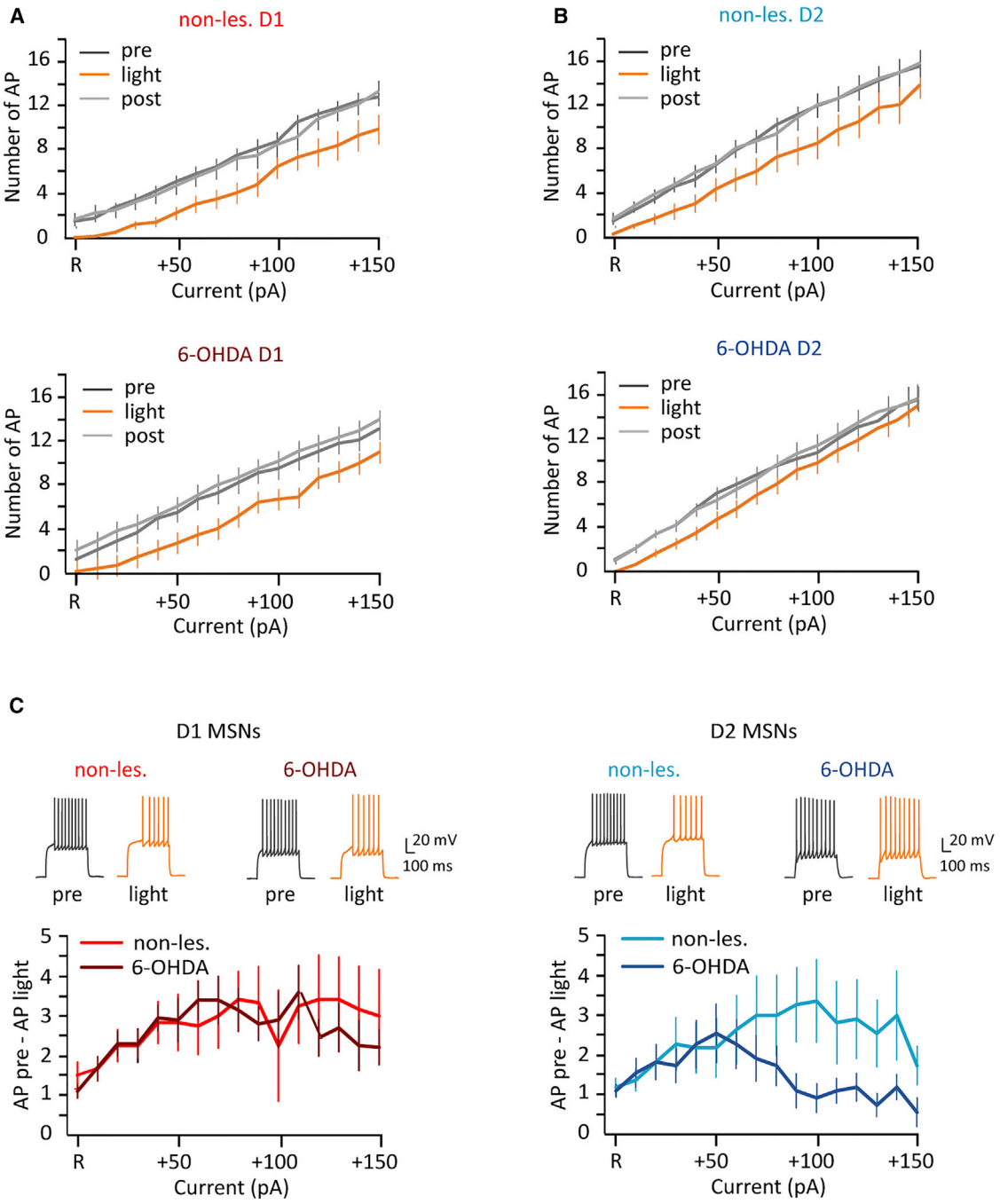

Figure 5. Photoinhibition of CINs Differentially Decreases D1 and D2 MSN Excitability in 6-OHDA Mice

(A and B) The graphs illustrate the decreased excitability of MSNs during light illumination versus pre and post conditions in non-lesioned (A, top; D1 MSNs: $F(2, 572) = 55.26$, $p < 0.0001$, $n = 12$; B, top; D2 MSNs: $F(2, 524) = 37.97$, $p < 0.0001$, $n = 11$, linear regression analysis) and 6-OHDA (A, bottom; D1 MSNs: $F(2, 953) = 209.72$, $p < 0.0001$, $n = 20$; B, bottom; D2 MSNs: $F(2, 524) = 17.09$, $p < 0.0001$, $n = 11$, linear regression analysis) mice. R is the minimal current intensity to trigger a spike in pre-light condition. From R, current intensity increased by +10-pA increment.

(C) (Top) Representative traces showing the responses to 500-ms depolarizing current steps (R+80 for D1 MSN non-les., D2 MSN non-les., and D2 MSN 6-OHDA) and R+110 (D1 MSN 6-OHDA). Light was delivered 200 ms before and continued 200 ms after the 500-ms depolarizing current step. (Bottom) The graphs show the difference in the number of action potentials evoked in pre versus light conditions in D1 MSNs (left; non-les., $n = 12$; 6-OHDA, $n = 20$) and D2 MSNs (right; non-les., $n = 11$; 6-OHDA, $n = 11$). There is a significant effect of current intensity in D1 MSNs ($F[15,450] = 3.67$, $p < 0.005$) and D2 MSNs ($F[15,300] = 2.02$, $p < 0.01$). From R+80 pA, D2 MSNs in 6-OHDA mice are less inhibited during light illumination, as shown by a significant interaction between lesion × current intensity for D2 MSNs ($F[15,300] = 2.39$, $p < 0.05$), but not for D1 MSNs. Errors bars, SEM.

inhibition linked to the activation of the direct (D1) pathway, but not the late excitation linked to the activation of the indirect (D2) pathway. The high degree of convergence of the direct pathway at the level of the SNr (48 striatal neurons converge into one SNr cell; Smith et al., 1998) may explain how a modest increase in corticostriatal transmission onto D1 MSNs impacts the cortically evoked inhibition in the SNr. In contrast, complex information processing at each stage of the polysynaptic indirect pathway might minimize the outcome of EPSC potentiation on D2 MSNs.

Another interesting result of our study is that DA depletion tends to erase the dichotomy in MSN excitability by inducing a specific increase in D1 MSN excitability. A recent study also reported increased D1 MSN excitability after DA lesion, but associated with a slight decrease in D2 MSN excitability (Fieblinger et al., 2014), whereas we failed to detect any change for D2 MSNs. This apparent discrepancy might be due to different lesion models or post-lesion delay, since opposite changes in D2 MSN excitability have been described after acute or chronic DA depletion (Day et al., 2006; Fieblinger et al., 2014; Shen et al., 2007). Elevated excitability in D1 MSNs might be considered as a homeostatic response counteracting the decreased activity triggered by the loss of dopaminergic excitatory drive on these neurons. However, if we assume that the dichotomy between D1 and D2 MSN excitability is a fundamental process for normal striatal function, making both MSNs more alike after DA depletion might be more harmful than beneficial. In favor of this hypothesis, we showed that CIN inhibition decreases the excitability more in D1 than in D2 MSNs after DA depletion, whereas it has similar impact on the two populations in control condition. Thus, restoring the dichotomy between D1 and D2 MSN excitability might be one component of the anti-parkinsonian effect of CIN inhibition. What happens following DA depletion to explain the reduced sensitivity of D2 MSNs to CIN inhibition remains an open and challenging question. It will be also interesting to investigate whether the cholinergic projection from the brainstem to the striatum (Dautan et al., 2014) cooperates with CINs to modulate striatal output.

Our results show that CINs are critical players in the host of cellular and synaptic changes induced in MSNs by DA depletion. Without excluding indirect pathway contributions, our findings point to CIN control of the direct striatonigral pathway as a critical component involved in the control of striatal output and motor dysfunction in PD state. These results should stimulate the development of therapeutic strategies targeting striatal CIN activity in PD.

EXPERIMENTAL PROCEDURES

Mice

All procedures were approved by the French National Ethical Committee (45-29102012) and were in accordance with the recommendations of the European Commission (2010/63/EU) for care and use of laboratory animals. See the Supplemental Experimental Procedures for a detailed description of the mice used.

Stereotaxic Surgery

All coordinates were adapted from the mouse stereotaxic atlas by Paxinos and Franklin (2001) with bregma and dura as references. See the Supplemental Experimental Procedures for details.

In Vitro Electrophysiology

Patch-clamp recordings on brain slices and data analysis were performed as described in the Supplemental Experimental Procedures. Excitation of opsins was achieved with a light-emitting diode source (Spectra light engine, Lumencor) connected to a 3-mm liquid core fiber. Statistical analyses were performed using paired or unpaired Student's t test. Nonparametric tests (Mann-Whitney test for unpaired data or Wilcoxon test for paired data) were used if the normality or equal variance test failed. For multiple group comparisons, one- or two-way ANOVA was used. We applied the log2 transformation to make the data normal if necessary. Linear regression analysis was used to compare the effect of CIN inhibition on MSN excitability. A significance of $p < 0.05$ was required for rejection of the null hypothesis.

Behavioral Testing

All behavioral analyses were conducted on littermates that entered the study at around 3–5 months of age. See the Supplemental Experimental Procedures for a detailed description of the behavioral tests. For open field, data were analyzed using two-way ANOVA followed by paired Student's t test, when appropriate. For haloperidol-induced catalepsy, median latencies (±semi-quartile) were compared among groups over time using the nonparametric Kruskal-Wallis test, followed by U-Mann-Whitney for pairwise comparisons at each time. Head movements were summed for the 3-min ON periods and compared to those measured 3-min OFF periods, using a two-way ANOVA. For cylinder and cross maze tests, data were analyzed using one-way ANOVA, followed by Student's t test. For L-DOPA-induced dyskinesia, data were analyzed by two-way repeated-measures (RM) ANOVA with opsins (eNpHR-RFP versus RFP) as between factor and time as within factor.

In Vivo Recordings in Anesthetized Mice

Extracellular recordings in the striatum and the SNr were performed as described in the Supplemental Experimental Procedures. The patterns of cortically evoked discharges in the same SNr neuron were analyzed before, during, and after CIN photoinhibition in the striatum. Results are given as means ± SEM of the individual responses per condition. Spontaneous activity in the three conditions was compared using one-way ANOVA followed by comparison versus pre-light condition (Holm-Sidak method). Cortically evoked responses of the same SNr neurons in the three light conditions were compared using one-way RM ANOVA, followed by comparison versus pre-light condition (Holm-Sidak method).

Histology and Immunohistochemistry

For primary antibody exposure, brain sections were incubated overnight at 4°C in rabbit anti-RFP (1/1,000, tebu-bio, 600-401-379) and goat anti-ChAT (1/100, Millipore, AB144P) for colocalization experiments and in mouse anti-tyrosine hydroxylase (1/1,000, Millipore, MAB318) to control DA lesion. Sections were then incubated, respectively, in Alexa Fluor 555 donkey anti-rabbit (1/500, Invitrogen, A31572), Alexa Fluor 488 donkey anti-goat (1/500, Invitrogen, A11055), and Alexa Fluor 555 donkey anti-mouse (1/500, Invitrogen, A31570) for 1 hr 30 min at room temperature. Rabbit anti-GFP (1/500, Invitrogen, A11122) and Alexa fluor 488 donkey anti-rabbit (1/500, Invitrogen, A21206) were used the same way to reveal eNpHR expression in transgenic mice.

SUPPLEMENTAL INFORMATION

Supplemental Information includes Supplemental Experimental Procedures, five figures, and two tables and can be found with this article online at http://dx.doi.org/10.1016/j.celrep.2015.09.034.

AUTHOR CONTRIBUTIONS

N.M., M.L., M.A., L.K.-L., and C.B. designed the study. N.M., M.L., F.J., S.Z., M.H., J.C., and C.B. performed experiments. K.D. provided reagents and critical feedback. N.M., M.L., F.J., S.Z., J.C., L.K.-L., M.A., and C.B. analyzed the results. N.M., M.L., M.A., L.K.-L., and C.B. wrote the paper.

ACKNOWLEDGMENTS

This work was supported by CNRS, Aix-Marseille Université, Fondation de France (2013 00043175), France Parkinson Association, and Agence Nationale de la Recherche (ANR-2010-1416). We thank C. Melon, C. Marra, and D. Paleressompoulle for their excellent technical assistance. Microscopy was performed at PiCSL-FBI core facility, member of the France-BioImaging national research infrastructure. We thank R. Ragheb, B. Burle, and P. Gubellini for statistical analysis; and A. Moqrich and P. Marcaggi for their critical comments on the manuscript.

Received: October 23, 2014
Revised: August 25, 2015
Accepted: September 10, 2015
Published: October 15, 2015

REFERENCES

Albin, R.L., Young, A.B., and Penney, J.B. (1989). The functional anatomy of basal ganglia disorders. Trends Neurosci. *12*, 366–375.

Aosaki, T., Graybiel, A.M., and Kimura, M. (1994). Effect of the nigrostriatal dopamine system on acquired neural responses in the striatum of behaving monkeys. Science *265*, 412–415.

Barbeau, A. (1962). The pathogenesis of Parkinson's disease: a new hypothesis. Can. Med. Assoc. J. *87*, 802–807.

Brown, P. (2003). Oscillatory nature of human basal ganglia activity: relationship to the pathophysiology of Parkinson's disease. Mov. Disord. *18*, 357–363.

Calabresi, P., Picconi, B., Tozzi, A., Ghiglieri, V., and Di Filippo, M. (2014). Direct and indirect pathways of basal ganglia: a critical reappraisal. Nat. Neurosci. *17*, 1022–1030.

Cui, G., Jun, S.B., Jin, X., Pham, M.D., Vogel, S.S., Lovinger, D.M., and Costa, R.M. (2013). Concurrent activation of striatal direct and indirect pathways during action initiation. Nature *494*, 238–242.

Dautan, D., Huerta-Ocampo, I., Witten, I.B., Deisseroth, K., Bolam, J.P., Gerdjikov, T., and Mena-Segovia, J. (2014). A major external source of cholinergic innervation of the striatum and nucleus accumbens originates in the brainstem. J. Neurosci. *34*, 4509–4518.

Day, M., Wang, Z., Ding, J., An, X., Ingham, C.A., Shering, A.F., Wokosin, D., Ilijic, E., Sun, Z., Sampson, A.R., et al. (2006). Selective elimination of glutamatergic synapses on striatopallidal neurons in Parkinson disease models. Nat. Neurosci. *9*, 251–259.

Degos, B., Deniau, J.M., Thierry, A.M., Glowinski, J., Pezard, L., and Maurice, N. (2005). Neuroleptic-induced catalepsy: electrophysiological mechanisms of functional recovery induced by high-frequency stimulation of the subthalamic nucleus. J. Neurosci. *25*, 7687–7696.

Ding, J., Guzman, J.N., Tkatch, T., Chen, S., Goldberg, J.A., Ebert, P.J., Levitt, P., Wilson, C.J., Hamm, H.E., and Surmeier, D.J. (2006). RGS4-dependent attenuation of M4 autoreceptor function in striatal cholinergic interneurons following dopamine depletion. Nat. Neurosci. *9*, 832–842.

English, D.F., Ibanez-Sandoval, O., Stark, E., Tecuapetla, F., Buzsáki, G., Deisseroth, K., Tepper, J.M., and Koos, T. (2011). GABAergic circuits mediate the reinforcement-related signals of striatal cholinergic interneurons. Nat. Neurosci. *15*, 123–130.

Eusebio, A., Thevathasan, W., Doyle Gaynor, L., Pogosyan, A., Bye, E., Foltynie, T., Zrinzo, L., Ashkan, K., Aziz, T., and Brown, P. (2011). Deep brain stimulation can suppress pathological synchronisation in parkinsonian patients. J. Neurol. Neurosurg. Psychiatry *82*, 569–573.

Fieblinger, T., Graves, S.M., Sebel, L.E., Alcacer, C., Plotkin, J.L., Gertler, T.S., Chan, C.S., Heiman, M., Greengard, P., Cenci, M.A., and Surmeier, D.J. (2014). Cell type-specific plasticity of striatal projection neurons in parkinsonism and L-DOPA-induced dyskinesia. Nat. Commun. *5*, 5316.

Galarraga, E., Hernández-López, S., Reyes, A., Miranda, I., Bermudez-Rattoni, F., Vilchis, C., and Bargas, J. (1999). Cholinergic modulation of neostriatal output: a functional antagonism between different types of muscarinic receptors. J. Neurosci. *19*, 3629–3638.

Gertler, T.S., Chan, C.S., and Surmeier, D.J. (2008). Dichotomous anatomical properties of adult striatal medium spiny neurons. J. Neurosci. *28*, 10814–10824.

Goldberg, J.A., Ding, J.B., and Surmeier, D.J. (2012). Muscarinic modulation of striatal function and circuitry. Handb. Exp. Pharmacol. *208*, 223–241.

Hernández-Echeagaray, E., Galarraga, E., and Bargas, J. (1998). 3-Alpha-chloro-imperialine, a potent blocker of cholinergic presynaptic modulation of glutamatergic afferents in the rat neostriatum. Neuropharmacology *37*, 1493–1502.

Higley, M.J., Gittis, A.H., Oldenburg, I.A., Balthasar, N., Seal, R.P., Edwards, R.H., Lowell, B.B., Kreitzer, A.C., and Sabatini, B.L. (2011). Cholinergic interneurons mediate fast VGluT3-dependent glutamatergic transmission in the striatum. PLoS ONE *6*, e19155.

Kravitz, A.V., Freeze, B.S., Parker, P.R., Kay, K., Thwin, M.T., Deisseroth, K., and Kreitzer, A.C. (2010). Regulation of parkinsonian motor behaviours by optogenetic control of basal ganglia circuitry. Nature *466*, 622–626.

Kreitzer, A.C., and Malenka, R.C. (2007). Endocannabinoid-mediated rescue of striatal LTD and motor deficits in Parkinson's disease models. Nature *445*, 643–647.

Lobb, C. (2014). Abnormal Bursting as a Pathophysiological Mechanism in Parkinson's Disease. Basal Ganglia *3*, 187–195.

Malenka, R.C., and Kocsis, J.D. (1988). Presynaptic actions of carbachol and adenosine on corticostriatal synaptic transmission studied in vitro. J. Neurosci. *8*, 3750–3756.

Mallet, N., Ballion, B., Le Moine, C., and Gonon, F. (2006). Cortical inputs and GABA interneurons imbalance projection neurons in the striatum of parkinsonian rats. J. Neurosci. *26*, 3875–3884.

Maurice, N., Deniau, J.M., Glowinski, J., and Thierry, A.M. (1999). Relationships between the prefrontal cortex and the basal ganglia in the rat: physiology of the cortico-nigral circuits. J. Neurosci. *19*, 4674–4681.

Nelson, A.B., Hammack, N., Yang, C.F., Shah, N.M., Seal, R.P., and Kreitzer, A.C. (2014). Striatal cholinergic interneurons Drive GABA release from dopamine terminals. Neuron *82*, 63–70.

Pakhotin, P., and Bracci, E. (2007). Cholinergic interneurons control the excitatory input to the striatum. J. Neurosci. *27*, 391–400.

Paxinos, G., and Franklin, K.B.J. (2001). The Mouse Brain in Stereotaxic Coordinates, Second Edition (San Diego: Academic Press).

Phelps, P.E., Houser, C.R., and Vaughn, J.E. (1985). Immunocytochemical localization of choline acetyltransferase within the rat neostriatum: a correlated light and electron microscopic study of cholinergic neurons and synapses. J. Comp. Neurol. *238*, 286–307.

Pisani, A., Bernardi, G., Ding, J., and Surmeier, D.J. (2007). Re-emergence of striatal cholinergic interneurons in movement disorders. Trends Neurosci. *30*, 545–553.

Rivlin-Etzion, M., Marmor, O., Heimer, G., Raz, A., Nini, A., and Bergman, H. (2006). Basal ganglia oscillations and pathophysiology of movement disorders. Curr. Opin. Neurobiol. *16*, 629–637.

Ryan, L.J., and Sanders, D.J. (1994). Subthalamic nucleus and globus pallidus lesions alter activity in nigrothalamic neurons in rats. Brain Res. Bull. *34*, 19–26.

Sano, H., Chiken, S., Hikida, T., Kobayashi, K., and Nambu, A. (2013). Signals through the striatopallidal indirect pathway stop movements by phasic excitation in the substantia nigra. J. Neurosci. *33*, 7583–7594.

Shen, W., Tian, X., Day, M., Ulrich, S., Tkatch, T., Nathanson, N.M., and Surmeier, D.J. (2007). Cholinergic modulation of Kir2 channels selectively elevates dendritic excitability in striatopallidal neurons. Nat. Neurosci. *10*, 1458–1466.

Smith, Y., Bevan, M.D., Shink, E., and Bolam, J.P. (1998). Microcircuitry of the direct and indirect pathways of the basal ganglia. Neuroscience *86*, 353–387.

Tachibana, Y., Kita, H., Chiken, S., Takada, M., and Nambu, A. (2008). Motor cortical control of internal pallidal activity through glutamatergic and GABAergic inputs in awake monkeys. Eur. J. Neurosci. *27*, 238–253.

Threlfell, S., Lalic, T., Platt, N.J., Jennings, K.A., Deisseroth, K., and Cragg, S.J. (2012). Striatal dopamine release is triggered by synchronized activity in cholinergic interneurons. Neuron *75*, 58–64.

Tritsch, N.X., Oh, W.J., Gu, C., and Sabatini, B.L. (2014). Midbrain dopamine neurons sustain inhibitory transmission using plasma membrane uptake of GABA, not synthesis. eLife *3*, e01936.

Wichmann, T., Bergman, H., Starr, P.A., Subramanian, T., Watts, R.L., and DeLong, M.R. (1999). Comparison of MPTP-induced changes in spontaneous neuronal discharge in the internal pallidal segment and in the substantia nigra pars reticulata in primates. Exp. Brain Res. *125*, 397–409.

Witten, I.B., Lin, S.-C., Brodsky, M., Prakash, R., Diester, I., Anikeeva, P., Gradinaru, V., Ramakrishnan, C., and Deisseroth, K. (2010). Cholinergic interneurons control local circuit activity and cocaine conditioning. Science *330*, 1677–1681.

Cell Reports

Supplemental Information

Striatal Cholinergic Interneurons Control Motor Behavior and Basal Ganglia Function in Experimental Parkinsonism

Nicolas Maurice, Martine Liberge, Florence Jaouen, Samira Ztaou, Marwa Hanini, Jeremy Camon, Karl Deisseroth, Marianne Amalric, Lydia Kerkerian-Le Goff, and Corinne Beurrier

SUPPLEMENTAL DATA

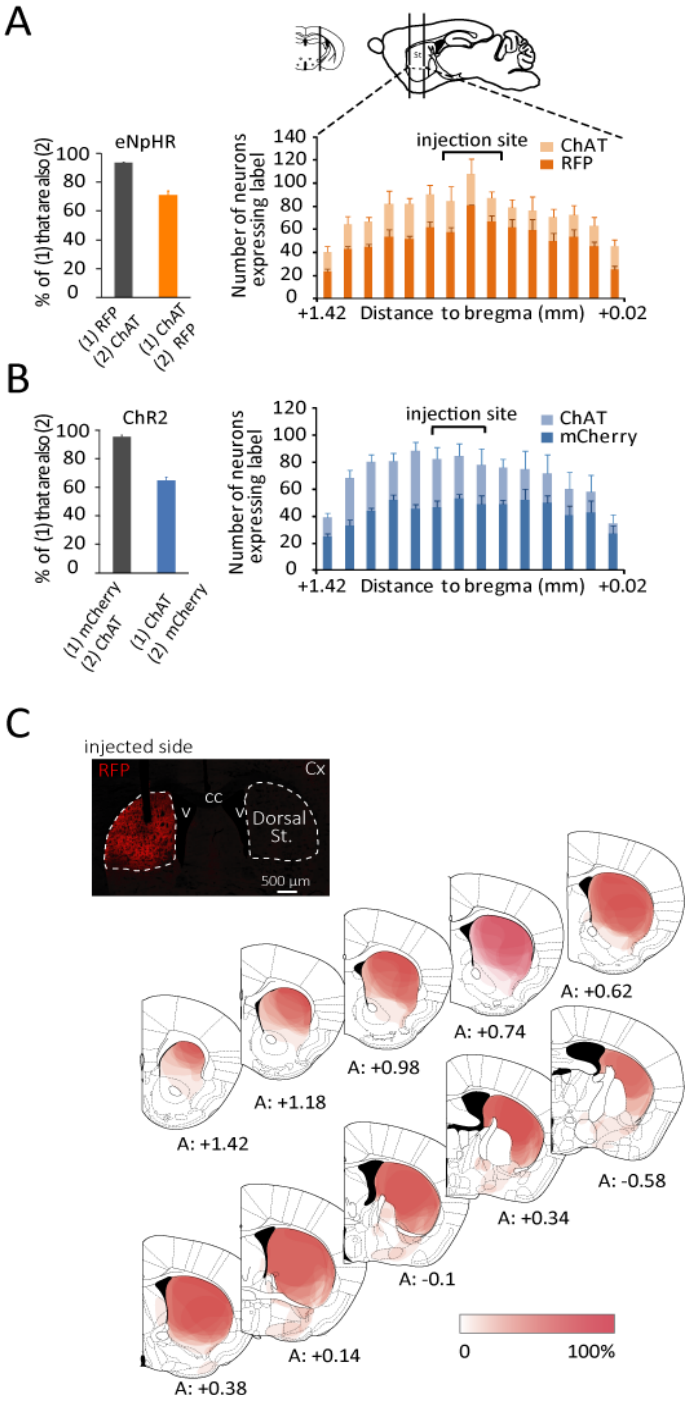

Figure S1, Related to Supplemental Experimental Procedures: Specific expression of opsins in CINs (A and B) and topography of RFP staining in eNpHR-RFP-injected mice (C).

(A, B) Left, histograms represent the mean coexpression in the whole dorsal striatum in eNpHR-RFP (n=2) or ChR2-mCherry (n=2) mice. Virtually all opsin-expressing neurons were ChAT-positive. The majority of neurons that expressed ChAT also expressed eNpHR-RFP (71.0 ± 2.9 %) or ChR2-mCherry (64.7 ± 2.6 %). Right, quantification of co-expression of RFP and mCherry and ChAT

immunofluorescence from two bilaterally eNpHR-RFP-injected and ChR2-mCherry-injected mice, from the rostral-to-caudal ends of the dorsal striatum (from +1.42 to +0.02 mm). Errors bars, SEM. (C) Top, coronal section showing a representative RFP staining from an eNpHR-RFP-injected mouse. The track shows the location at which viral injection, followed by implantation of optical fiber, was made. Note the large diffusion of eNpHR-RFP in nearly the whole dorsal striatum. Cx: cortex, cc: corpus callosum, v: ventricle, St: striatum. Bottom, coronal schematic sections from the stereotaxic atlas of Paxinos and Watson showing the topography of RFP staining in eNpHR-RFP mice (from +1.42 to -0.58 mm with bregma as reference, n=14 mice). The intensity of the gradient of color (white to red) corresponds to the measured RFP positive area in the different brain structures studied for each injection performed. The highest intensity of red (100%) indicates that all animals had signal in the corresponding area, whereas the lowest color intensity (white, 0%) corresponds to non-stained areas. RFP labeling outside the striatum was very scarce and localized ventrally in the nucleus accumbens or caudally in the ventral pallidum and the bed nucleus of the stria terminalis.

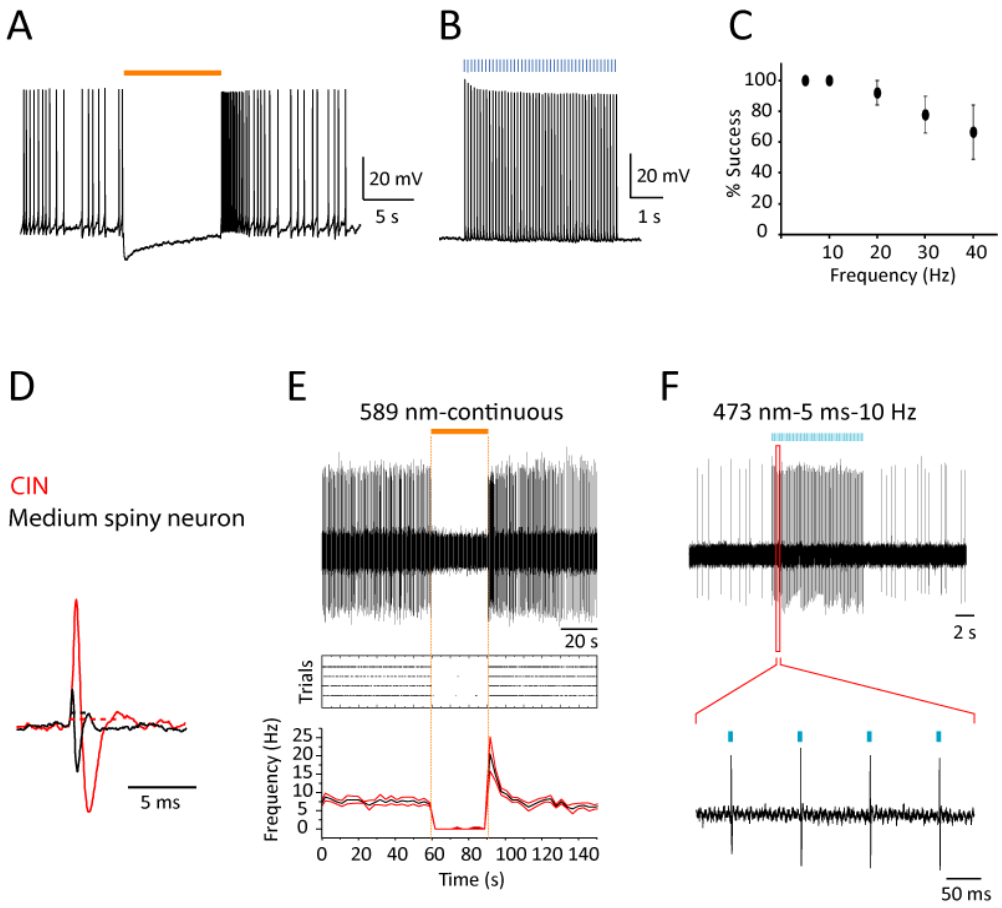

Figure S2: Functional expression of ChR2-mCherry and eNpHR-RFP in CINs both *in vitro* (A, B and C) and *in vivo* (D, E and F).

(A) Action potential inhibition induced by 10 s yellow light illumination in a eNpHR-RFP-expressing neuron. (B) Action potentials in a ChR2-mCherry-expressing neuron evoked by 5-ms blue light pulses (10 Hz). (C) Average success probability for generating action potentials in neurons expressing ChR2-mCherry at different stimulation frequencies (n=4-5, 5-ms pulse width). (D) Superimposed recordings of a CIN and a medium spiny neuron. CINs were distinguished from medium size spiny neurons by their typical tonic activity and spike duration. Dotted lines indicate spike duration. (E) Raw trace (top) of an isolated unit, identified as a CIN, inhibited by yellow light continuous stimulation. Raster plot (middle) displaying the response of the same unit to four repetitions of the light stimulation, with each action potential represented as a dot. Average and SEM of the firing rate over time (bottom) for the same unit. (F) Raw trace (top) of another putative CIN that is excited by 5ms-blue light pulses (10 Hz). Note at higher magnification that every light pulse drives a spike (bottom). Errors bars, SEM.

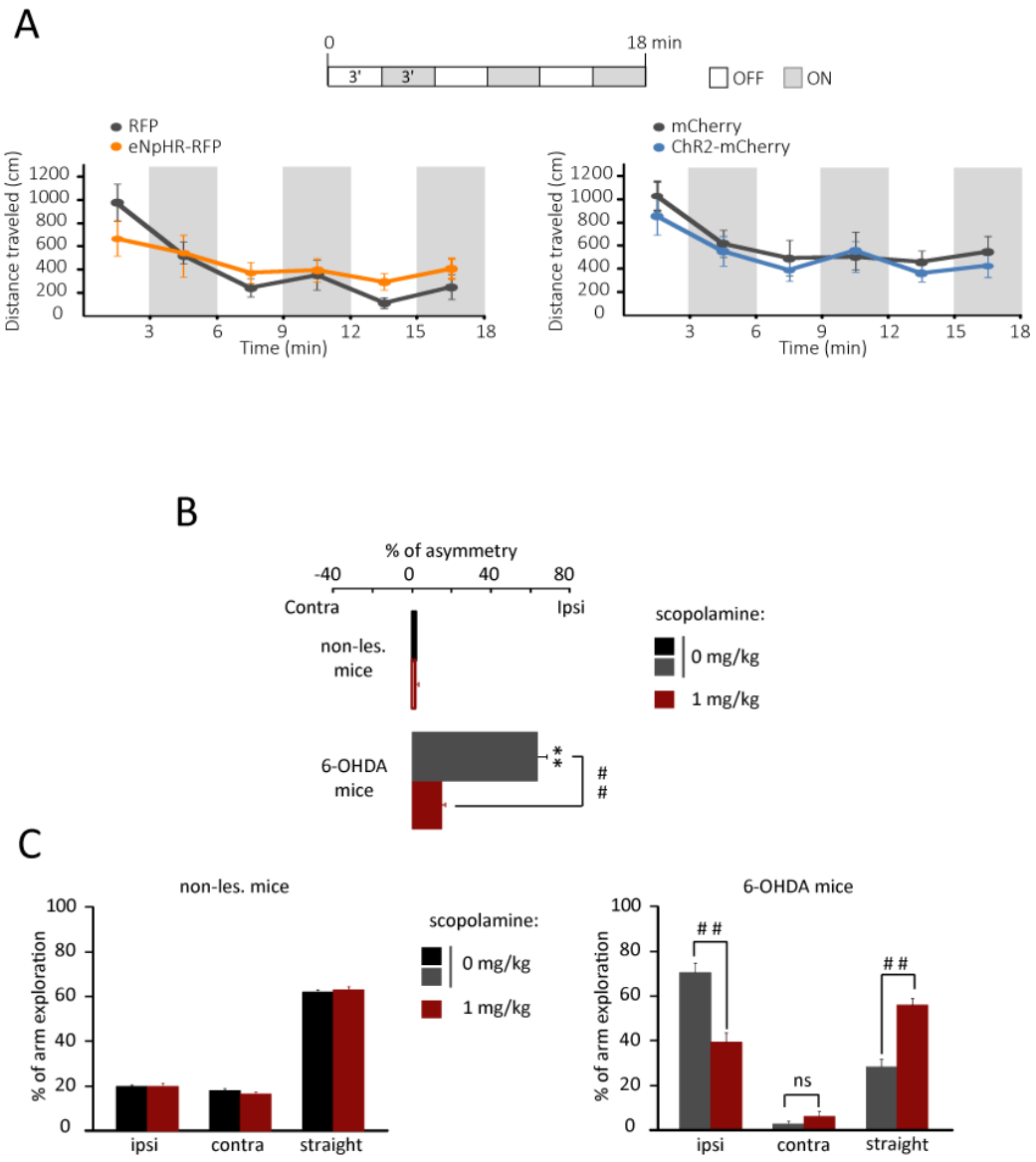

Figure S3, related to Figure 1: (A) Effects of CIN manipulation on the spontaneous locomotor activity in non-lesioned mice. Top, experimental design. Graphs show the locomotor activity before (OFF) and during (ON) bilateral striatal illumination in RFP, eNpHR-RFP, mCherry and ChR2-mCherry mice, in 3-min period. No change in ambulation was observed in response to photoinhibition or photoactivation of CINs in either group (two-way ANOVA, ns), n=6-9 per group. (B, C) Muscarinic receptors blockade with scopolamine relieves parkinsonian-like motor deficits. B, in the cylinder test, 6-OHDA mice (n=14) showed a marked forelimb asymmetry compared to non-lesioned mice (*p<0.01, Fisher PLSD test after significant ANOVA $F_{3,40}$=76.66). This asymmetry was significantly improved by intraperitoneal (i.p.) scopolamine injection (scopolamine 1 mg/kg vs. 0 mg/kg: # p<0.01, Student's *t* test). Scopolamine did not affect asymmetry in non-lesioned mice (n=8). C, non-lesioned mice (n=8) placed in the cross-maze perform mainly straight-arm exploration with equivalent percentage of ipsi- or contralateral arms

exploration (*p<0.01, Fisher PLSD test after significant ANOVA $F_{5,35}$=402.9). 6-OHDA lesion induced a bias in arms exploration with a dramatic increase in ipsilateral turns and decrease in contralateral and straight exploration. Scopolamine significantly modified the performance of 6-OHDA mice (n=14) in the cross-maze (significant one-way ANOVA $F_{5,65}$=48.58, p<0.01). It significantly decreased ipsilateral arm exploration ($^{\#}$ p<0.01, Student's *t* test) and increased straight exploration ($^{\#}$ p<0.01, Student's *t* test) while not affecting contralateral bias (ns, Student's *t* test). Errors bars, SEM.

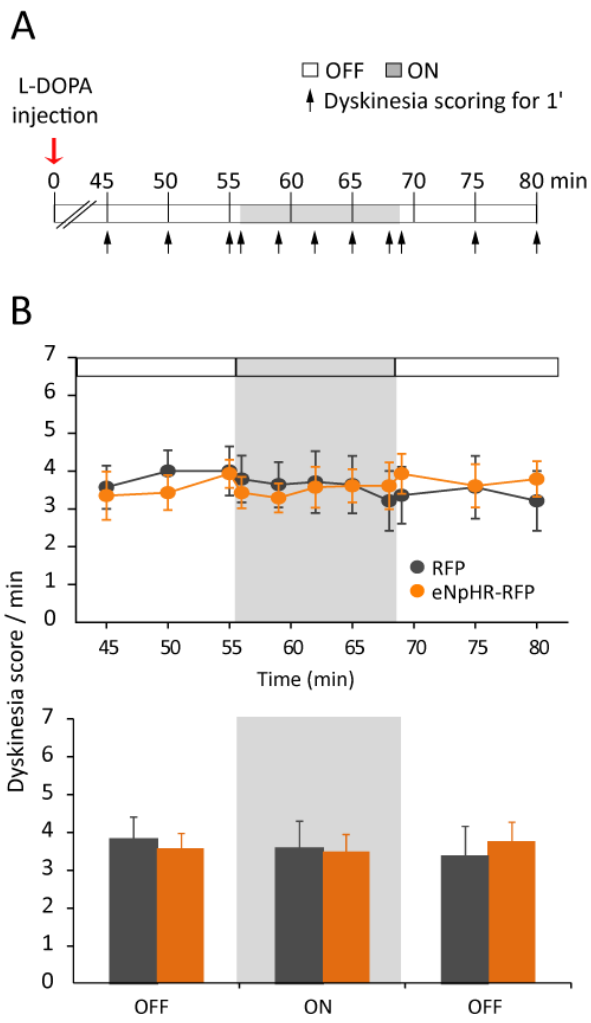

Figure S4: Photoinhibition of CINs does not affect L-DOPA-induced dyskinesia.

(A) Experimental design. Two weeks after intranigral injection of 6-OHDA, RFP and eNpHR-RFP mice received a chronic L-DOPA treatment for 21 days and dyskinesia were quantified at day 21. (B) Time profile of dyskinesia score (sum of the mean scores for axial and forelimb dyskinesia over 35 min; maximum score 8) after L-DOPA injection on day 21 of chronic treatment. Light did not produce a significant difference in dyskinesia score (two-way repeated measure ANOVA, ns, n = 7 per group). Errors bars, SEM.

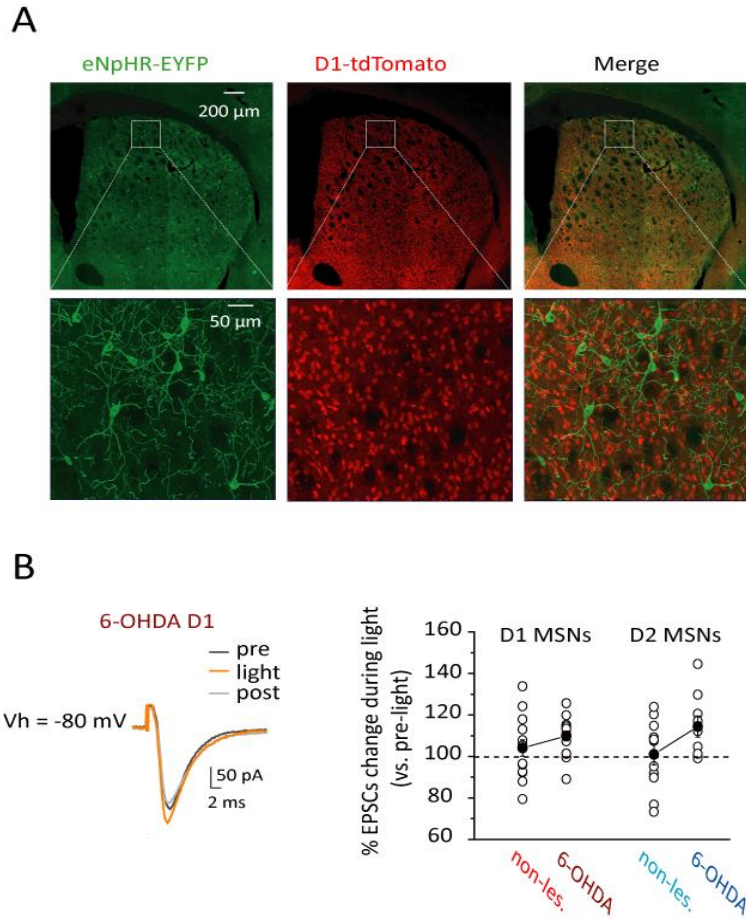

Figure S5, related to Figures 4 and 5: (A) Representative photomicrographs of a transgenic eNpHR/D1 mouse. Dorsal striatum sections showing eNpHR-EYFP expressing cells that are immunostained with antibodies against GFP (green) and D1-MSNs which are visualized by the direct fluorescence of tdTomato (red). Merge image shows no colocalization. (B) Photoinhibition of CINs potentiates corticostriatal transmission onto both populations of MSNs in 6-OHDA mice. EPSCs traces from a D1 MSN recorded in a 6-OHDA mouse before, during and after light illumination. Light was sent 50 ms before cortical stimulation and continue 250 ms after. Graph illustrates the value of EPSCs change during light illumination compared to pre-light condition in all cells. Black circles represent the mean. Errors bars, SEM.

	Frequency of discharge (Hz)		Burst recurrence (burst/s)		Burst duration (s)		Number of spikes/burst	
	Non-lesioned (n = 18)	**6-OHDA (n = 13)**	Non-lesioned	**6-OHDA**	Non-lesioned	**6-OHDA**	Non-lesioned	**6-OHDA**
Pre	14.4 ± 1.7	**12.3 ± 1.4**	0.218 ± 0.057	**0.258 ± 0.070**	0.384 ± 0.033	**0.517 ± 0.052***	9.5 ± 0.6	**14.0 ± 1.1****
Light	13.2 ± 1.8	**11.1 ± 1.5**	0.247 ± 0.053	**0.315 ± 0.068**	0.398 ± 0.036	**0.374 ± 0.031#**	9.4 ± 0.5	**9.5 ± 0.5##**
Post	13.0 ± 1.7	**11.9 ± 2.1**	0.255 ± 0.046	**0.290 ± 0.075**	0.460 ± 0.030	**0.404 ± 0.028**	10.6 ± 0.5	**11.9 ± 0.6**

Table S1, related to Figure 2: Effect of 6-OHDA lesion and impact of CIN photoinhibition on spontaneous activity of SNr neurons in transgenic eNpHR mice.

* p<0.05, ** p<0.01, unpaired Student's *t* test, 6-OHDA *vs.* non-lesioned mice. #p<0.05, ##p<0.01, one-way ANOVA followed by Holm-Sidak post-hoc test, *vs.* pre-light condition.

		Early excitation			Inhibition		Late excitation		
		L (ms)	D (ms)	Nb Sp	L (ms)	D (ms)	L (ms)	D (ms)	Nb Sp
Non-lesioned	Pre-Light	11.0 ± 0.9 (n = 13)	7.5 ± 0.7	45.5 ± 8.3	22.8 ± 1.2 (n = 18)	25.4 ± 3.2	45.1 ± 3.4 (n = 13)	8.5 ± 1.0	44.0 ± 6.3
	Light	10.9 ± 0.9	8.1 ± 1.2	47.6 ± 7.7	21.8 ± 1.1	25.4 ± 3.9	43.9 ± 3.4	9.2 ± 1.2	44.9 ± 7.1
	Post-Light	11.5 ± 0.8	8.7 ± 0.8	54.0 ± 8.8	22.0 ± 1.2	25.3 ± 2.4	44.0 ± 2.3	9.6 ± 1.0	47.5 ± 8.6
6-OHDA	**Pre-Light**	**11.0 ± 2.5 (n = 6)**	**9.0 ± 2.9**	**60.3 ± 13.4**	**22.3 ± 1.5 (n = 9)**	**23.0 ± 4.3**	**58.0 ± 7.1 (n = 10)**	**33.8 ± 5.9**	**133.4 ± 32.1**
	Light	**10.0 ± 3.0**	**8.0 ± 2.5**	**55.0 ± 17.1**	**19.3 ± 1.7**	**36.3 ± 6.4****	**62.2 ±10.2**	**35.8 ± 9.2**	**137.6 ± 26.7**
	Post-Light	**10.0 ± 2.6**	**9.3 ± 2.1**	**50.0 ± 23.3**	**20.0 ± 2.6**	**32.4 ± 4.8**	**61.2 ± 8.5**	**38.2 ± 4.8**	**119.2 ± 32.4**

Table S2, related to Figure 2: Characteristics of the responses evoked on the same SNr cells by electrical stimulation of the motor cortex in non-lesioned and 6-OHDA transgenic eNpHR mice, before, during and following CINs photoinhibition.

The latency (L) and duration (D) of the different components of the cortically evoked response were measured on the basis of post-stimulus time histograms generated from 100 cortical stimulations. Nb Sp: number of spikes of the excitatory component.

**p≤0.01, one-way repeated measure ANOVA followed by Holm-Sidak post-hoc test, *vs.* pre-light condition.

SUPPLEMENTAL EXPERIMENTAL PROCEDURES

Mice. All mice strains used in this study were purchased from Jackson Laboratory. We used Choline acetyltransferase ChAT-IRES-Cre knock-in mice ($ChAT^{cre/cre}$ mice, stock number: 006410), LoxP-stop-eNpHR3.0-EYFP mice (Ai39 mice, stock number: 014539) and BAC Drd1a-tdTomato mice ($Tg^{D1\text{-}tdTomato}$ mice, stock number: 016204). Ai39 mice were crossed with $ChAT^{cre/cre}$ mice to induce eNpHR3.0 expression in cholinergic neurons and were used for *in vivo* electrophysiology ($Rosa^{eNpHR/+}$::$ChAT^{cre/+}$ mice that were called transgenic eNpHR mice in this study). For *in vitro* electrophysiological experiments requiring distinguishing D1 and D2 MSNs, $Rosa^{eNpHR/+}$::$ChAT^{cre/+}$ mice were crossed with $Tg^{D1\text{-}tdTomato}$ mice to obtain both eNpHR expression in the cholinergic neurons and dtTomato expression in the direct(D1)-MSNs ($Rosa^{eNpHR/+}$::$ChAT^{cre/+}$::$Tg^{D1\text{-}tdTomato}$ mice that were called transgenic eNpHR/D1 mice in this study) (Figure S5).

Stereotaxic surgery. Mice were anaesthetized with intraperitoneal (i.p.) injections of ketamine and xylazine (100 and 10 mg/kg, respectively) and mounted on a stereotaxic apparatus (Kopf Instruments). Injections were made with a 10-µl syringe, connected to the injector by a polyethylene tubing, and controlled by an injection pump at 0.3 µl/min.

Viral expression of opsins in CINs. pAAV vectors containing opsins transgenes (ChR2: pAAV-Ef1a-DIO-hChR2(H134R)-mCherry and eNpHR: pAAV-Ef1a-DIO-eNpHR3.0-EYFP) were provided by Dr. Deisseroth (Stanford University). For practical consideration, we switched EYFP by TagRFP by overlap extension PCR cloning method. The recombinant AAV vectors were serotyped with AAV5 coat proteins and packaged by the viral vector core at the University of North Carolina. To achieve Cre-dependent expression of opsins in CINs, we microinjected 1 µl of AAV at two dorso-ventral sites into the dorsal striatum of $ChAT^{cre/cre}$ mice (+1.0 mm AP, ±1.5 mm ML, -2.7 and -2.1 mm DV). Opsin-expressing neurons were largely confined to the dorsal striatum (Figure S1B). Mice that were used in behavioral experiments were then implanted with a bilateral guide cannula (+1.0 mm AP, ± 1.5 mm ML, 26 gauge, positioned 2.5-mm below skull; PlasticsOne). All viral injections were made unilaterally except for *in vitro* recordings and haloperidol-induced catalepsy.

6-OHDA lesions. Mice received one unilateral injection of 6-OHDA hydrochloride (1.5 µl at 2.7 µg/µl diluted in 0.9% sterile NaCl containing 0.1% ascorbic acid, Sigma-Aldrich) into the substantia nigra pars compacta: -3.0 mm AP, ±1.3 mm ML, -4.3 mm DV. 6-OHDA injection was immediately followed by unilateral intrastriatal viral injection and experiments were performed at least two weeks later. DA lesion extent was systematically assessed by anti-tyrosine hydroxylase immunochemistry.

Optic fiber implantation. For L-DOPA-induced dyskinesia experiments that required long-term treatment, we used implantable optical fibers consisting of a zirconia ferrule with a 200-µm diameter

and 3.3 mm-long cleaved bare optic fibers (0.22 N.A., Doric Lenses). Fibers were implanted ipsilaterally to the lesioned side at the following coordinates: +1.0 mm AP, ± 1.5 mm ML, -2.0 mm DV.

***In vitro* electrophysiology.** Coronal striatal slices (250 µm) from 7 to 10-week-old bilaterally AAV-injected or transgenic mice were cut in ice-cold high-choline artificial cerebro-spinal fluid (ACSF) with a vibratome (Leica) as previously described (Beurrier et al., 2009). Recordings from 6-OHDA mice were performed 2 to 3 weeks after 6-OHDA injection and the extent of DA lesion was systematically assed a posteriori by anti-tyrosine hydroxylase immunochemistry in the striatum. Only mice exhibiting >70% of DA depletion compared to the non-injected hemisphere were kept for the analysis. Slices were then transferred to oxygenated ACSF and maintained at room temperature until recording. Neurons were visualized on an upright microscope (Nikon Eclipse FN1) equipped with DIC optic and filters set to visualize mCherry, TagRFP, tdTomato and EYFP using a x40 water-immersion objective. Combination of electrophysiological properties and expression of fluorophore was used to identify CINs and D1 MSNs while unlabeled MSNs were considered as D2 MSNs. Recordings were interleaved in labeled D1 MSNs and unlabeled putative D2 MSNs from the same mice. Patch-clamp recordings were performed in cell-attached and whole-cell configurations in current- or voltage-clamp mode in oxygenated ACSF warmed to 33°C. Patch-clamp electrodes (4-6 MΩ) were filled with an intracellular solution containing 126 mM $KMeSO_4$, 14 mM KCl, 3 mM $MgCl_2$, 0.5 mM $CaCl_2$, 5 mM EGTA, 10 mM HEPES, 2 mM NaATP and 0.5 mM NaGTP, pH adjusted to 7.25 with NaOH and osmolarity adjusted to 270-280 mOsm/L. To activate opsins, light was delivered under control of the acquisition software from a Spectra Light Engine (Lumencor, Optoprim) and was focused onto the back aperture of the microscope objective, producing a wide-field exposure around the recorded cell.

MSN excitability was tested at least 5 min after seal rupture by sending a series of 500 ms depolarizing current steps with an increment of 10 pA. For trials in which CINs were photoinhibited, light was ON 200 ms before and continue 200 ms after the 500 ms depolarizing current step, making the total illumination time equal to 900 ms. The time interval between each current step was 3 s. EPSCs were elicited by current pulses (0.1-ms width every 10 s) using a bipolar tungsten electrode placed preferentially at the motor cortex-dorsal striatum border to stimulate afferents from the motor cortex. For trials in which CINs were photoinhibited, light was ON 50 ms before cortical stimulation and continues 250 ms after. EPSCs amplitudes were calculated on at least 10 averaged traces by taking a mean of a 1-ms window around the peak and comparing this with the mean of a 3-ms window immediately before the stimulation artifact. Series resistances were monitored with a 5-mV negative step given with every afferent stimulus. Data were collected with a MultiClamp 700B amplifier (Molecular Devices), analyzed and plotted in clampfit (Molecular Devices, v 10.2) and Origin (v 7.5).

Behavioral testing. *Open-field.* Spontaneous locomotor activity was evaluated in an open field placed in a dim lighted room. Before testing, mice were acclimated to the testing room for at least 1 h. RFP, eNpHR-RFP, mCherry and ChR2-mCherry mice were tested for 18 min in a square chamber (50 x 50 cm) with a 30 cm-high white plastic wall. CINs were photoactivated (25-ms pulse width, 10 Hz) or photoinhibited (continuous illumination) during 3-min ON periods interspersed with 7-min OFF periods. Ambulation was defined as the total distance (in cm) covered by each mouse measured by 3-min bin for 18 min and recorded by a video track system (Viewpoint Life sciences Inc.).

Haloperidol-induced catalepsy. Optical fibers were inserted into the bilateral cannula just before haloperidol injection. Mice received 0.25 mg/kg haloperidol i.p. After 20 min, mice forepaws were placed on an horizontal bar 4 cm above the floor and the latency to step down was measured (with a cut-off of 120 s) every 10 min during the 80-min test (Figure 1A). Head movements were also measured continuously for the whole test duration. Mice received either blue (25-ms pulse width, 10 Hz) or yellow (continuous illumination) light 20 min after haloperidol injection. Light was ON for 3-min during which catalepsy was measured and then turned OFF for 7 min until the next measurement started.

Cylinder test. Mice were put into Plexiglas cylinders (20 cm height, 9 cm diameter) in order to evaluate motor asymmetry induced by 6-OHDA lesion. The number of contacts against the cylinder wall with the forepaws (weight-bearing contacts with fully extended digits) was monitored continuously for 5 min by two investigators blind of experimental conditions. A double contact was defined as simultaneous or closely performed ipsilateral and contralateral forepaws touches. Mice failing to reach 10 contacts were excluded from the analyses. Data are expressed as side bias calculated as % ipsilateral minus % contralateral contacts to the 6-OHDA lesioned side. All mice were tested only once to prevent habituation to the apparatus. Two groups of eNpHR-RFP or ChR2-mCherry 6-OHDA-lesioned mice were tested either in ON or OFF condition (yellow light: continuous illumination for 5 min, blue light: 25-ms pulse width, 10 Hz) and compared to the non-lesioned group. The same experiment was performed in two groups of RFP or mCherry 6-OHDA mice.

Cross maze test. Mice were placed into a cross maze consisting of 4 identical arms (45 cm × 7 cm × 15 cm) at 90° to each other and made with clear Plexiglas. The acquisition sessions started with the mouse placed in the middle, facing one arm. The number of ipsilateral and contralateral turns as well as the number of time the mouse went straight was monitored for 5 min. Pre-6-OHDA data were collected and then, 2 weeks after 6-OHDA lesions, mice were tested twice: one to collect post-6-OHDA data without light and the day after with the light ON (yellow light: continuous illumination for 5 min, blue light: 25-ms pulse width, 10 Hz).

L-DOPA-induced dyskinesia. Fifteen to eighteen days after 6-OHDA injections, mice received a single daily injection of L-DOPA (20 mg/kg) and benserazide hydrochloride (10 mg/kg) for 21 days. The abnormal involuntary movements (AIMs) were assessed by two investigators blind of subject viral

infections (eNpHR-RFP or RFP). Peak-dose dyskinesia scoring was performed for 1 min at different time points, 45 to 80 min after the last L-DOPA injection on day 21 (Figure S4). Axial and limb AIMs were scored using a previously established scale from 0 to 4 for each AIM subtype (Lundblad et al., 2004) and the sum of the 2 scores, defined as dyskinesia score, was determined for each animal (maximal score, 8). Yellow light was delivered during 13 min, starting 56 min after L-DOPA injections.
For experiments involving scopolamine injection (scopolamine hydrobromide, Sigma-Aldrich), scopolamine was dissolved with NaCl and administered by i.p. injection at a dose of 1 mg/kg in $ChAT^{cre/cre}$ mice.

Optogenetic photostimulation and photoinhibition in awake mice. Optical fiber (200 µm- diameter, 0.22 N.A., Doric Lenses) was inserted without anesthesia through the implanted cannula (tip protruding 0.3 mm). For bilateral illumination, optical fibers were connected to the laser through a rotary joint (FRJ_1x2i_FC-2FC, Doric Lenses) that sent half of the light coming from the laser into each of the two optical fibers inserted in the mouse brain and enabled the mouse to move freely during behavioral assessments. Light was provided by a yellow- (589 nm, 75.2 mW) and blue- (473 nm, 118.5 mW) laser (Combined Dual Wavelength DPSS Laser System, Laserglow). Optical-fiber light power was measured using a light sensor and intensity calculated using the model based on direct measurements in mammalian brain tissue for predicting irradiance values developed in K. Deisseroth's lab and available at http://www.stanford.edu/group/dlab/cgi-bin/graph/chart.php. Light intensity at 0.2 mm from fiber tip was calculated to be 11.3 and 20.0 mW/mm^2 for blue and yellow light, respectively (corresponding to 200 and 140 mW/mm^2 at the fiber tip).

***In vivo* recordings in anaesthetized mice.** Non-lesioned and 6-OHDA lesioned (at least two weeks post-lesion) transgenic eNpHR mice were anesthetized with a mixture of ketamine and xylazine (100 and 10 mg/kg i.p., respectively, supplemented as needed by i.p. injection during the course of the experiment) and fixed in a stereotaxic head frame (Horsley-Clarke apparatus; Unimécanique). Body temperature was monitored by a rectal thermometer and maintained at 36.5°C with a homeothermic blanket (Harvard Apparatus). Single-unit activity of SNr cells was recorded extracellularly using glass micropipettes (25-35 MΩ) filled with a 0.5 M sodium chloride solution containing 1.5 % neurobiotin (Vectors Laboratories Inc.). Single neuron action potentials were recorded using the active bridge mode of an Axoclamp-2B amplifier (Molecular Devices), amplified, and filtered with an AC/DC amplifier (DAM 50; World Precision Instruments). Nigral neurons were identified as non-dopaminergic by their classically defined electrophysiological characteristics: narrow spikes (width ≤ 2 ms) and ability to present relatively high frequency discharges (> 10 Hz) without decrease in spike amplitude (Deniau et al., 1978). The optical fiber (core 200 µm, N.A. 0.22, Dorics Lenses) was positioned in the striatum (+1.0

mm AP, ±1.5 mm ML, -2.0 mm DV). The cortical and SNr areas to stimulate and record, respectively, were precisely defined by anterograde and retrograde tracing methods consisting in an iontophoretic deposit, at these striatal coordinates, of wheat germ agglutinin horseradish peroxydase (Vector Laboratories). This striatal territory receives inputs from the motor cortical area stimulated (+2.1 mm AP, ±0.5 mm ML, -0.7 mm DV) and sends projections to the recording site in the SNr (-3.3 mm AP, ±1.5 mm ML, -4.0/-4.8 mm DV). The patterns of cortically-evoked responses in the same SNr neuron were analyzed before, during and after CIN photoinhibition in the striatum. Yellow light was delivered for 5 min (589 nm, power at the tip of optical fiber: 140 mW/mm^2). Only SNr cells presenting an inhibitory component in response to cortical stimulation were recorded as they were the only ones to receive direct inputs from the striatal area activated by cortical stimulation meaning they belonged to the basal ganglia channel in register with the cortical area stimulated. This inhibitory component was preceded and/or followed by excitations due to the activation of the two trans-subthalamic pathways. Population post-stimulus time histograms (PSTHs) were generated by aligning the evoked responses on the onset of the inhibitory component. Results are given as means ± SEM of the individual responses per condition.

Spontaneous activity of SNr neurons was analyzed before, during and after CIN photoinhibition in the striatum by sampling a period of 60 s in each condition. Yellow light was delivered for 5 min (589 nm, power at the tip of optical fiber: 140 mW/mm^2). Epochs of elevated discharge rate were classified as bursts using a Poisson Surprise analysis (Legendy and Salcman, 1985). This was done using a script written for the Spike2 software. Briefly, this analysis evaluates how improbable any given burst, that contains n spikes in a time interval T, occurred by chance and computed as follows: S = -log p, where p is the probability that, in a random (Poisson) spike train having the same average spikes rate r as the spike train studied, a given time interval of length T contains n or more spikes. p is given by Poisson's formula, as follows:

$$p = e^{-rT} \sum_{i=n}^{\infty} (rT)^i / i!$$

where S refers to the Poisson Surprise of the burst (the degree to which the burst surprises a person who expects the spike train to be a Poisson process). In this study, only spike trains with S $\geqslant$ 2 were considered to be bursts. At the end of electrophysiological experiments, the tip of the stimulating electrodes was marked by an electrical deposit of iron (5 µA anodal, 20 s) and the tip of the recording electrodes was marked by iontophoretic ejection of Chicago Sky Blue (Sigma, 4% in NaCl 0,6 M; 8 µA cathodal, 20 min). Brains were removed and fixed in a 10% formalin solution after a ferri-ferrocyanide reaction. The localization of the blue points and iron deposits were observed on serial frozen sections (70 µm) counterstained with safranin O (Sigma). All the recorded cells kept in the analysis were localized in the SNr.

Histology, immunohistochemistry and microscopy. Animals were deeply anesthetized with a mixture of ketamine/xylazine and then transcardially perfused with an ice-cold solution of paraformaldehyde 4% in PBS. After dissection, brains were post-fixed overnight in the same fixative at 4 °C, cryoprotected in 30% sucrose dissolved in 1X PBS for an additional 36 h at 4 °C, and frozen. Coronal cryostat sections (40 µm) covering the antero-posterior extent of the striatum or the substantia nigra pars compacta were used for labeling. Brain sections were permeabilized in PBS with 0.4% Triton X-100 (PBST) for 30 min at room temperature. Sections were then incubated in a blocking solution composed of PBST with 3% bovine serum albumin and 10% normal goat serum for 1h at room temperature. Immunostaining was done on free-floating sections, which were then mounted onto SuperFrost Plus glass slides (VWR) and coverslipped with FluorSave mounting media (Merck Chemicals). Quantification of colocalization was performed from approximately bregma +1.42 to +0.02 mm (around 14 sections per mouse) using Mercator System (Explora Nova) combined with a DMR Leica microscope coupled to a DXC-990P color video camera (Sony). Images were collected using Axio Imager Z1 with the Apotome system (Zeiss) with a Plan-Apochromat 20×/0.8 or a Plan-Neofluar x40/1.3 objective (Zeiss) for the high magnification or with a Plan-Apochromat 10×/0.45 objective (Zeiss) to acquire whole-brain images.

SUPPLEMENTAL REFERENCES

Beurrier, C., Lopez, S., Révy, D., Selvam, C., Goudet, C., Lhérondel, M., Gubellini, P., Kerkerian-LeGoff, L., Acher, F., Pin, J.-P., et al. (2009). Electrophysiological and behavioral evidence that modulation of metabotropic glutamate receptor 4 with a new agonist reverses experimental parkinsonism. FASEB J. *23*, 3619–3628.

Deniau, J.M., Hammond, C., Riszk, A., and Feger, J. (1978). Electrophysiological properties of identified output neurons of the rat substantia nigra (pars compacta and pars reticulata): evidences for the existence of branched neurons. Exp. BRAIN Res. *32*, 409–422.

Kolomiets, B.P., Deniau, J.M., Glowinski, J., and Thierry, A.M. (2003). Basal ganglia and processing of cortical information: functional interactions between trans-striatal and trans-subthalamic circuits in the substantia nigra pars reticulata. Neuroscience *117*, 931–938.

Legendy, C.R., and Salcman, M. (1985). Bursts and recurrences of bursts in the spike trains of spontaneously active striate cortex neurons. J. Neurophysiol. *53*, 926–939.

Lundblad, M., Picconi, B., Lindgren, H., and Cenci, M.A. (2004). A model of L-DOPA-induced dyskinesia in 6-hydroxydopamine lesioned mice: relation to motor and cellular parameters of nigrostriatal function. Neurobiol. Dis. *16*, 110–123.